Interfacial Reaction during Friction Stir Welding of Al and Cu

Cécile Genevois, Marion Girard, Bertrand Huneau, Xavier Sauvage, Guillaume Racineux

Interfacial Reaction during Friction Stir Welding of Al and Cu

C. GENEVOIS, M. GIRARD, B. HUNEAU, X. SAUVAGE, and G. RACINEUX

Commercially pure copper was joined to a 1050 aluminum alloy by friction stir welding. A specific configuration where the tool pin was fully located in the aluminum plate was chosen. In such a situation, there is no mechanical mixing between the two materials, but frictional heating gives rise to a significant thermally activated interdiffusion at the copper/aluminum interface. This gives rise to the formation of defect-free joints where the bonding is achieved by a very thin intermetallic layer at the Cu/Al interface. Nanoscaled grains within this bonding layer were characterized using transmission electron microscopy (TEM). Two phases were identified, namely, Al_2Cu and Al_4Cu_9 phases. The nucleation and growth of these two phases are discussed and compared to the standard reactive interdiffusion reactions between Cu and Al.

I. INTRODUCTION

WELDING dissimilar metals with different chemical, mechanical, or thermal properties has always been a challenging issue but is still of great interest for many applications such as in chemical, nuclear, aerospace, transportation, power generation, and electronics industries. The friction stir welding (FSW) process is now a well-established joining process, and it has been demonstrated that high quality welds can be achieved in aluminum,[1–4] magnesium,[5] steel,[6,7] and copper[8–12] alloys. FSW is a solid-state joining process; it is therefore a promising technique to achieve defect-free dissimilar welds. It has been shown indeed that it could be successfully applied to weld dissimilar Al alloys,[13] aluminum to magnesium,[14,15] aluminum to steel,[16] or aluminum to copper.[17–23] Copper and aluminum are widely used in engineering applications where a combination of high electrical or thermal conductivity, corrosion, and mechanical properties is required. One should note, however, that welding copper is intrinsically difficult by conventional welding processes because of its high thermal conductivity. For the same reason, defect-free joints are difficult to achieve by FSW and low welding speeds together with high rotational rates are usually required.[8–12] Probably also for the same reason, welding copper to aluminum by FSW often leads to defected joints with many cracks and cavities.[22] Some authors managed to find a small window of optimum processing parameters,[19,20,22] but in all cases, thick layers of brittle intermetallic compounds (IMCs) were formed. Aluminum and copper have indeed a strongly negative mixing enthalpy leading to the easy formation of intermetallic phases that are brittle.[18–20,24]

During FSW in butt joint configuration, the stirring pin is usually located on the butt line to achieve a strong mixing between materials of the two plates. However, for dissimilar welding, some authors have recently shown that both the position of the pin and the selection of the metal positioned on the advancing side may strongly influence the quality of the joint.[13,14,16,17,25–29] For example, Lee and Jung managed to obtain void-free welds between a 6061 aluminum alloy and copper only by shifting the stirring pin toward the aluminum plate.[17]

In the present study, a 1050 aluminum alloy was joined to commercially pure copper (99.9 pct) following this approach. However, to avoid the formation of a thick layer of brittle IMCs, positioning the stirring pin fully in the aluminum plate is proposed. The bonding between the two metals is achieved only by reactive interdiffusion resulting from the frictional heating. This method is called friction stir diffusion bonding.

II. EXPERIMENTAL PROCEDURE

Plates (4-mm thickness) of 1050-H16 aluminum alloy and commercially pure copper Cu-b1 (equivalent to UNS C12200 H01 (1/4 hard)) were friction stir welded using a computer numerically controlled milling machine. This machine is controlled in position with a gantry configuration. The tool rotational speed and travel speed were 900 rpm and 100 mm/min, respectively. The welding direction was parallel to the rolling direction of the plates. The copper plate, which was the harder material, was on the advancing side and the aluminum alloy plate on the retreating side. Unlike the conventional friction stir butt welding, the unthreaded tool pin was positioned in the aluminum plate, tangentially to the copper plate in order to reduce the mixing between both materials and, thus, the formation of brittle intermetallic phases.

C. GENEVOIS, Engineer of Research, and X. SAUVAGE, Research Scientist, are with the Groupe de Physique des Matériaux, Faculté des Sciences, University of Rouen, CNRS UMR 6634, 76801 Saint-Etienne du Rouvray, France. Contact e-mail: cecile.genevois@univ-rouen.fr M. GIRARD, Associated Researcher, B. HUNEAU, Assistant Professor, and G. RACINEUX, Professor, are with the Institut de Recherche en Génie Civil et Mécanique, CNRS UMR 6183, Ecole Centrale de Nantes, 44321 Nantes, France.

Vickers microhardness tests were performed on the cross section perpendicular to the welding direction using a Future-Tech 7E micromet (Testwell S.A., St Ouen, France), with a 100 g load for 15 seconds. Microstructural changes from the weld zone to the unaffected base metal were observed by optical microscopy using an Olympus BX51M microscope (Olympus SAS, Rungis, France). Specimens were prepared in the weld cross sections. They were first mechanically polished and then anodized at 26 V for 80 seconds (10 mL HBF4 + 200 mL distilled water) to reveal the grain structure on the aluminum side under polarized light. The microstructure on the Cu side was observed after chemical etching (1 mL $FeCl_3$ + 10 mL HCl + 30 mL ethanol). The Al/Cu interface was observed by scanning electron microscopy (SEM) in secondary electron mode using a NVision microscope (Zeiss, Nanterre, France). The sample was mechanically polished before observation.

Base materials and welds were also characterized using transmission electron microscopy (TEM). Samples (3-mm disc) were punched out from various locations in the weld and in the original plates. These latter samples were first mechanically thinned down to 100 μm and then electropolished using a Tenupol 3 (Struers, Champigny sur Marne, France) with a nitric acid/methanol solution at 248 K (–25 °C) and a voltage of 12 V (15 V, respectively) for aluminum (copper, respectively). Samples selected in the weld were mechanically thinned down to 50 μm in thickness, and electron transparency was obtained by ion milling (GATAN PIPS). TEM observations were carried out on JEOL* 2000FXII and JEOL 2100 microscopes operating at 200 kV. Elemental compositions were analyzed by scanning transmission electron microscopy–energy-dispersive spectroscopy (STEM-EDS) and energy filtered transmission electron microscopy (EFTEM) (GIF-GATAN, Gatan, Evry, France) imaging on the JEOL 2100 microscope.

*JEOL is a trademark of Japan Electron Optics Ltd., Tokyo.

III. RESULTS AND DISCUSSION

The copper base material exhibits equiaxed grains with an average diameter of 20 μm. On the optical micrograph (Figure 1(a)), large twins are also observed, while TEM observations revealed a significant dislocation density (Figure 1(b)) probably resulting from rolling. The microhardness of the copper plate is 81 ± 2 HV.

The aluminum base material exhibits a typical rolling microstructure with elongated-pancake grains (about 200-μm long and 10-μm large) with a dense substructure.

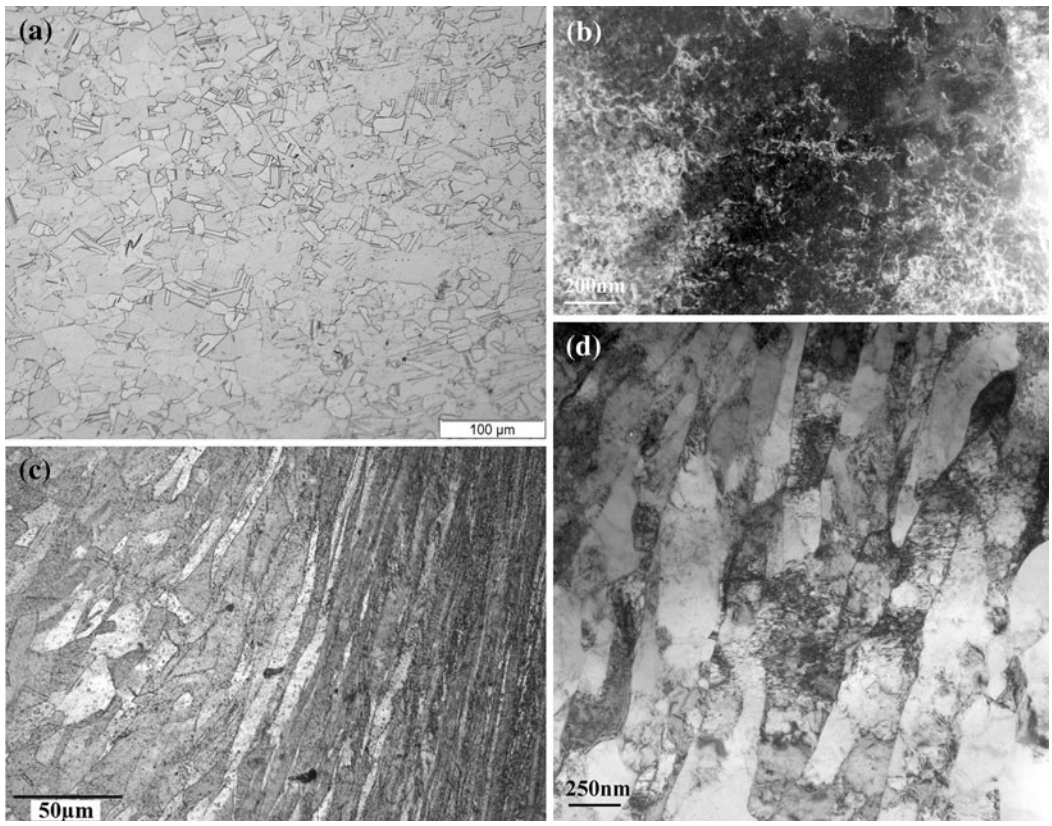

Fig. 1—Observations of different regions on the copper side of the Al-Cu joint produced by friction stir welding: (*a*) optical micrograph of the grain structure and twins in the copper base material, (*b*) TEM bright field of the dislocation organization in the copper base material, (*c*) rotated and elongated grains close to the Al/Cu interface, and (*d*) bright-field TEM micrograph showing the grain and the dislocation structures in the TMAZ in the copper side, close to the Al/Cu interface.

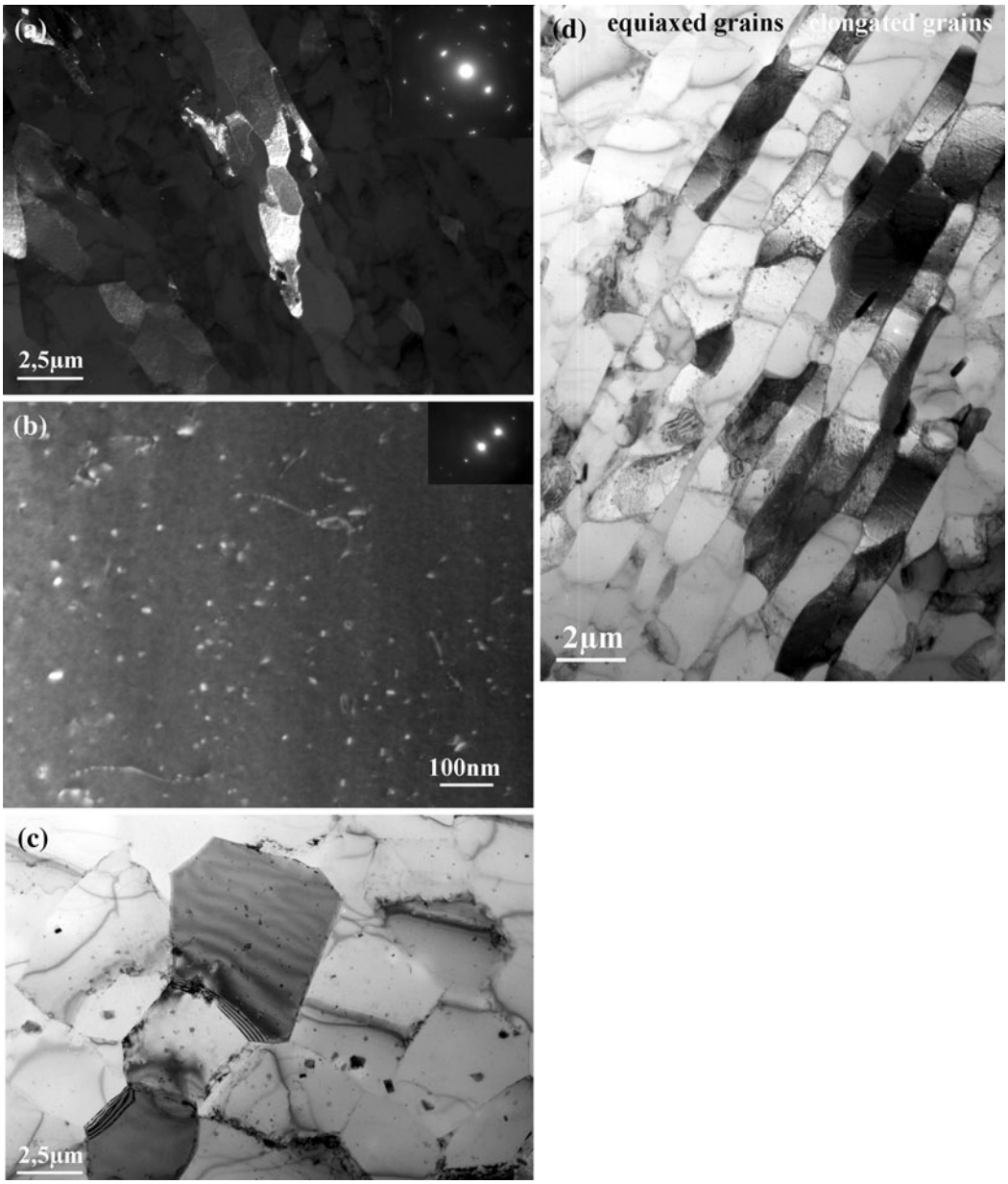

Fig. 2—TEM micrographs showing the microstructure in different regions of the weld on the aluminum side: (*a*) dark field with $g = (200)$, subgrain structure in the base material; (*b*) weak beam dark field with $g = (200)$ showing the dislocations population; (*c*) bright field showing the microstructure in the stir zone; and (*d*) bright field of the grain structure in the TMAZ. The elongated grains present a subgrain structure with dislocations and the equiaxed grains contain very low dislocation density.

The average size of the subgrains is about 1.3 μm in diameter (Figure 2(a)). There are a few linear dislocations, but numerous dislocation loops could be observed (Figure 2(b)). The microhardness of the aluminum plate is 44 $\pm$ 2 HV, significantly lower than the copper plate.

Figure 3 shows the SEM micrograph of a typical defect-free weld cross section obtained with the previously described welding conditions. Since the tool was shifted toward the Al alloy, the stirring action of the pin took place mainly in the aluminum alloy and, as expected, the Al/Cu interface does not exhibit apparent mechanical mixing.

The hardness profile recorded along the centerline of the cross section (Figure 4) clearly shows that there is a thin layer at the Cu/Al interface, the hardness of which is up to 125 $\pm$ 2 HV. In the nugget (exclusively located on the Al side), the hardness is slightly lower than that of the original plate (down to 35 $\pm$ 2 HV) and the profile is rather typical of friction stir welds of non-heat-treatable aluminum alloy welded in the strain-hardened state.[30] The three different regions can be identified (Figure 4): the stir zone or nugget, the unaffected parent material, and a transition region in-between (thermomechanically affected zone (TMAZ)). On the Cu side, there are only two regions: the parent material and a hardened region near the interface with a steep hardness gradient.

In the nugget (exclusively located on the Al side due to the applied welding conditions), grains are equiaxed

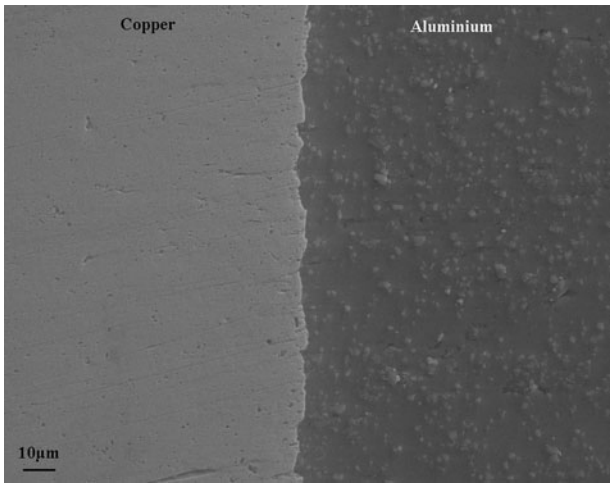

Fig. 3—SEM micrograph (SE mode) of the defect-free Al/Cu junction.

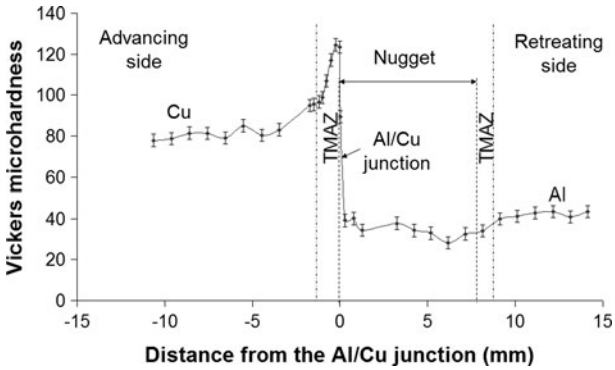

Fig. 4—Vickers microhardness profile measured along the centerline of the cross section of the weld. The advancing side was situated on the pure copper and the retreating side on the aluminum alloy.

(average diameter of 5 μm), and the dislocation density (including loops) is very low (Figure 2(c)). These features clearly indicate that dynamic recrystallization occurred and is consistent with the observed drop of hardness in the nugget (Figure 4). Indeed, the strength of aluminum alloys from the 1XXX series is predominantly controlled by work hardening and the grain size. TEM micrographs show that the dislocation density is very low in the stir zone and the base material. Moreover, the grain size of the stir zone ($\approx$5 μm in diameter) is slightly bigger than the subgrain size of the base material ($\approx$1.5 μm in diameter). This may explain the softening observed in the weld nugget. The small second-phase particles (darker particles) exhibited in the stir zone (Figure 2(c)) were analyzed by energy dispersive X-ray spectroscopy (data not shown here). They contain Al, Fe, and Mn and are $Al_6(Mn,Fe)$ intermetallics.[31] It is interesting to note that the size of the recrystallized region is larger than the pin diameter (7.8 ± 0.1 *vs* 6.6 ± 0.1 mm). This indicates that there is some material flow and heat transfer at a significant distance to the pin. This feature will be further discussed later.

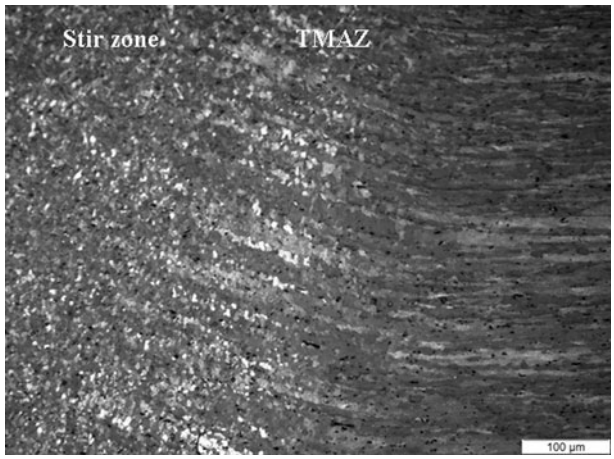

Fig. 5—Optical micrograph showing the evolution of the grain structure through the stir zone –TMAZ regions in the aluminum side.

The TMAZ between the stir zone and the base metal of the aluminum plate (Figure 5) is quite narrow (about 200 μm). This feature is attributed to the unthreaded pin used for welding. The extent of plastic deformation is indeed usually limited with this kind of tool.[32] The TMAZ exhibits both original grains that were tilted and elongated by the plastic flow (4-μm long with an aspect ratio of about 3) and small equiaxed grains (about 2 μm in diameter) with a low dislocation density (Figure 2(d)).

The maximum hardness was recorded on the copper side in a 300-μm-thick region layering the Al/Cu interface. In this layer, grains are strongly elongated and aligned along the plastic flow direction resulting from the pin motion (Figures 1(c) and (d)). At a distance of 100 μm of the Al/Cu interface, the grain rotation is close to 70 deg. Thus, this region exhibits a similar structure compared to the TMAZ on the Al side, and the high hardness, up to 125 HV, close to the interface can be attributed to the strain hardening of copper.

Since the pin was located exclusively on the Al side, such heavy deformation of the copper was not expected. It is also worth noticing that, usually, TMAZ of copper friction stir welds does not exhibit such tilted and elongated grains.[8,10] Although there is no mixing between copper and aluminum in the present welding conditions, one should admit that the pin tool has induced a significant level of plastic flow also on the copper side. This plastic deformation was transmitted into the copper by friction of the aluminum flowing along the Al/Cu interface prior to the reaction discussed in the following.

TEM observations carried out in various locations of the weld along the Al/Cu interface show a thin layer of nanoscaled grains (Figure 6(a)). This layer is 200-nm thick, on average, but exhibits noticeable irregularities especially at the bottom of the weld where some fragmentation was observed (data not shown here). The EFTEM image (Figure 6(b)) shows that the layer is divided into two sublayers referred to as layer A close on the aluminum side and layer B on the copper side in the following. These two layers contain some copper and

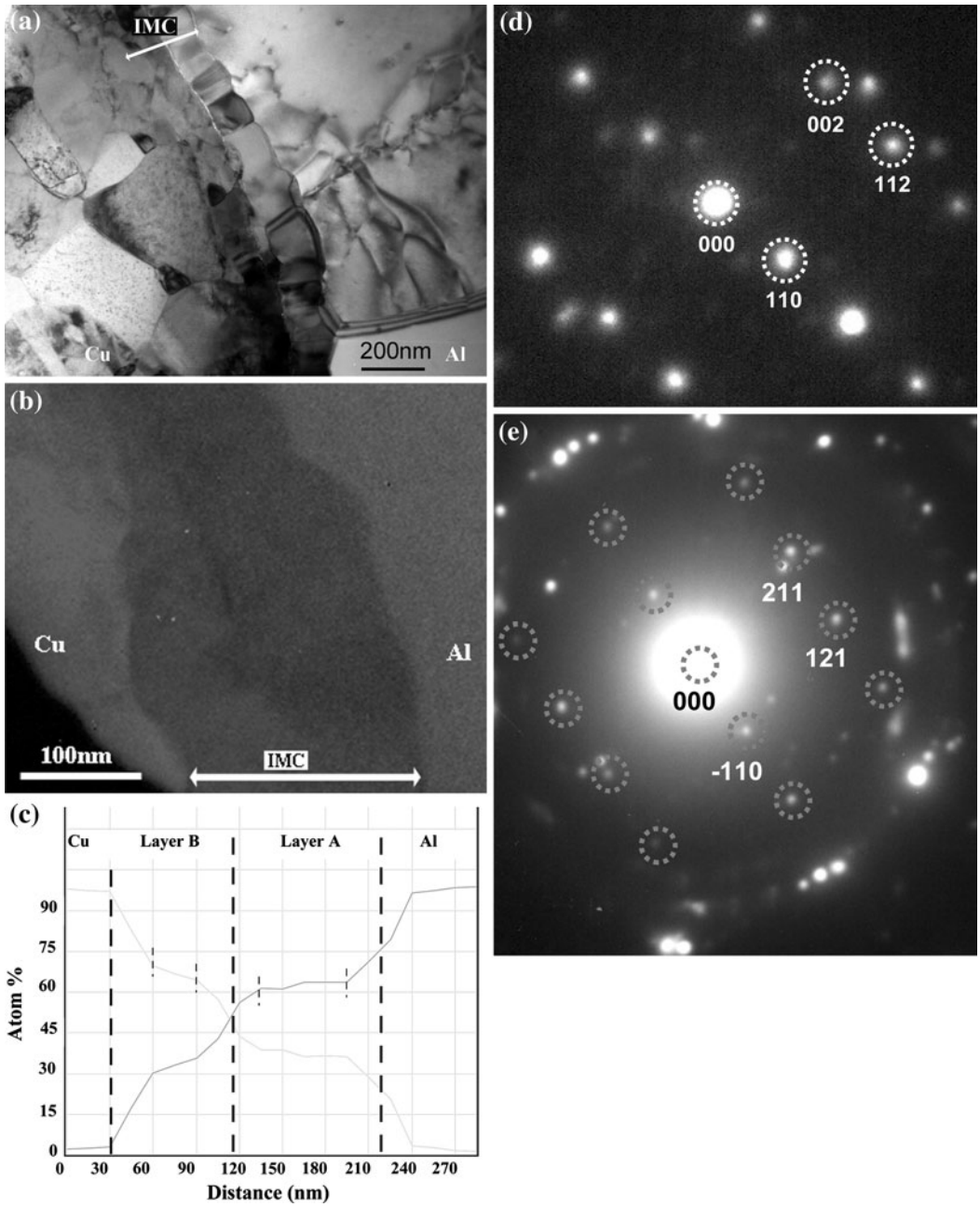

Fig. 6—TEM observations and STEM analysis across the Al/Cu interface of the weld. (*a*) TEM bright field showing the intermetallic compound grains at the Al/Cu interface. (*b*) EFTEM image showing two layers with a different chemical composition at the Al/Cu interface. It was obtained by selecting the aluminum element and the copper element. (*c*) STEM-EDS profile showing the evolutions of the aluminum and copper concentrations across the Al/Cu interface. (*d*) SAED pattern of a grain situated in the intermetallic compound layer close to the aluminum side (layer A). It showed the[1–10] zone axis of the Al_2Cu phase (θ). (*e*) SAED pattern of a grain situated in the layer close to the copper side (layer B). It showed the [11-3] zone axis of the Al_4Cu_9 phase (γ).

aluminum but in different ratios; thus, they might be attributed to two different IMCs. The layer A is a one-grained thick layer where grains are equiaxed (average size of about 120 nm) and boundaries are sharp. The layer B is thinner (average thickness of about 80 nm) with a grain structure that is not well defined. However, it is interesting to note that these IMCs layers are rather regular and do not exhibit deformation features. Since the grain structure on the copper side close to the Al/Cu interface is significantly deformed (Figure 1(d)), one may reasonably assume that the IMC layers have nucleated and grown once the pin tool left the area (*i.e.*, when the local plastic flow was down to almost zero).

According to selected area electron diffraction (SAED) patterns, layer A is the body-centered-tetragonal Al_2Cu (θ) intermetallic compound and layer B is the cubic Al_4Cu_9 (γ) intermetallic compound (Figures 6(d) and (e)). Line scans by energy-dispersive X-ray analyses show the evolution of the mean chemical composition

through these two nanolayers (Figure 6(c)). In layer A (on the Al side), the average chemical composition is 63 at. pct Al and 37 at. pct Cu (1 pct uncertainty), while that of layer B (on the Cu side) ranges between 64.4 and 69.6 at. pct Cu and 35.6 and 30.4 at. pct Al (1 pct uncertainty). This latter phase has a larger composition gradient than the Al_2Cu (θ) compound, which is consistent with the equilibrium phase diagram.[33] These measurements are also in agreement with the data reported for Al-Cu dissimilar welding by classical FSW,[19,20,22] where Al_2Cu (θ) and Al_4Cu_9 (γ) are the main IMCs observed. According to the effective heat of formation model,[33,34] the phase Al_2Cu (θ) is expected to nucleate first followed by AlCu (η) and then Al_4Cu_9 (γ). The AlCu (η) phase was observed by Xue *et al.* in Al-Cu nuggets[35] but was not detected in the present investigation, where EFTEM analyses did not exhibit a third layer between the Al_2Cu (θ) and the Al_4Cu_9 (γ). Thus, one may assume that in the IMC layers of the present study, the AlCu (η) phase nucleated first but was then fully transformed into Al_4Cu_9 (γ) during the temperature decrease that occurs in the material after the welding process.[36]

IV. CONCLUSIONS

A 1050 aluminum alloy was successfully welded to commercially pure copper by friction stir welding. The pin tool was located exclusively on the Al side, and there was no mixing of either material through the weld. The bonding results only from reactive interdiffusion; therefore, this process is named friction stir diffusion bonding. The reactive interdiffusion of Al and Cu gives rise to the formation of a very thin layer of intermetallic compounds at the Al/Cu interface (about 200 nm only). Extensive microstructure analyses by TEM indicate that this layer was formed after the stirring action of the tool pin (*i.e.*, once the pin tool left). Two intermetallics compounds were detected, namely, the Al_2Cu (θ) and Al_4Cu_9 (γ) phases.

ACKNOWLEDGMENT

The authors gratefully acknowledge Dr. R. Ravelle-Chapuis, JEOL SAS, for TEM analysis on the JEOL 2100 microscope.

REFERENCES

1. K.V. Jata, K.K. Sankaran, and J.J. Ruschau: *Metall. Mater. Trans. A*, 2000, vol. 31A, pp. 2181–92.
2. Y.S. Sato, H. Kokawa, M. Enomoto, and S. Jogan: *Metall. Mater. Trans. A*, 1999, vol. 30A, pp. 2429–37.
3. J.Q. Su, T.W. Nelson, R. Mishra, and M. Mahoney: *Acta Mater.*, 2003, vol. 51, pp. 713–29.
4. C. Genevois, A. Deschamps, A. Denquin, and B. Doisneau-Cottignies: *Acta Mater.*, 2005, vol. 53, pp. 2447–58.
5. D. Zhang, M. Suzuki, and K. Maruyama: *Scripta Mater.*, 2005, vol. 52, pp. 899–903.
6. Y.S. Sato, T.W. Nelson, C.J. Sterling, R.J. Steel, and C.O. Pettersson: *Mater. Sci. Eng.*, 2005, vol. A397, pp. 376–84.
7. H. Fujii, L. Cui, N. Tsuji, M. Maeda, K. Nakata, and K. Nogi: *Mater. Sci. Eng.*, 2006, vol. A 429, pp. 50–57.
8. C.G. Andersson and R.E. Andrews: *Proc. 1st Int. Symp. on Friction Stir Welding*, Thousand Oaks, CA, June 14–16, 1999.
9. C.G. Andersson, R.E. Andrews, B.G.I. Dance, M.J. Russell, E.J. Olden, and R.M. Sanderson: *Proc. 2nd Int. Symp. on Friction Stir Welding,* Gothenburg, Sweden, June 26–28, 2000.
10. W.-B. Lee and S.-B. Jung: *Mater. Lett.*, 2004, vol. 58, pp. 1041–46.
11. H.S. Park, T. Kimura, T. Murakami, Y. Nagano, K. Nakata, and M. Ushio: *Mater. Sci. Eng.*, 2004, vol. A 371, pp. 160–69.
12. G.M. Xie, Z.Y. Ma, and L. Geng: *Scripta Mater.*, 2007, vol. 57, pp. 73–76.
13. P. Cavaliere and F. Panella: *J. Mater. Process. Technol.*, 2008, vol. 206, pp. 249–55.
14. J. Yan, Z. Xu, Z. Li, L. Lei, and S. Yang: *Scripta Mater.*, 2005, vol. 53, pp. 585–89.
15. A.C. Somasekharan and L.E. Murr: *Mater. Charact.*, 2004, vol. 52, pp. 49–64.
16. H. Uzun, C. Dalle Donne, A. Argagnotto, T. Ghidini, and C. Gambaro: *Mater. Des.*, 2005, vol. 26, pp. 41–46.
17. W.B. Lee and S.B. Jung: *Mater. Res. Innov.*, 2003, vol. 8, pp. 93–96.
18. W.B. Lee, K.S. Bang, and A.B. Jung: *J. Alloys Compd.*, 2005, vol. 390, pp. 212–19.
19. J. Ouyang, E. Yarrapareddy, and R. Kovacevic: *J. Mater. Process. Technol.*, 2006, vol. 172, pp. 110–22.
20. A. Abdollah-Zadeh, T. Saeid, and B. Sazgari: *J. Alloys Compd.*, 2008, vol. 460, pp. 535–38.
21. P. Liu, Q. Shi, W. Wang, X. Wang, and Z. Zhang: *Mater. Lett.*, 2008, vol. 62, pp. 4106–08.
22. T. Saeid, A. Abdollah-zadeh, and B. Sazgari: *J. Alloys Compd.*, 2010, vol. 490, pp. 652–55.
23. M. Girard, B. Huneau, C. Genevois, X. Sauvage, and G. Racineux: *Sci. Technol. Weld. Join.*, 2010, vol. 15 (8), pp. 661–65.
24. M. Abbasi, A. Karimi Taheri, and M.T. Salehi: *J. Alloys Compd.*, 2001, vol. 319, pp. 233–41.
25. R.S. Coelho, A. Kostka, J. dos Santos, and A.R. Pyzalla: *Adv. Eng. Mater.*, 2008, vol. 10 (12), pp. 1127–33.
26. W.B. Lee, M. Schmuecker, U. Alfaro Mercardo, G. Biallas, and S.-B. Jung: *Scripta Mater.*, 2006, vol. 55, pp. 355–58.
27. T. Tanaka, T. Morishige, and T. Hirata: *Scripta Mater.*, 2009, vol. 61, pp. 756–59.
28. T. Watanabe, H. Takayama, and A. Yanagisawa: *J. Mater. Process. Technol.*, 2006, vol. 178, pp. 342–49.
29. C.M. Chen and R. Kovacevic: *Int. J. Mach. Tools Manuf.*, 2004, vol. 44, pp. 1205–14.
30. M. Peel, A. Steuwer, M. Preuss, and P.J. Withers: *Acta Mater.*, 2003, vol. 51, pp. 4791–4801.
31. Y.S. Sato, S.H.C. Park, and H. Kokawa: *Metall. Mater. Trans. A*, 2001, vol. 32A, pp. 3033–42.
32. H.R. Shercliff and P.A. Colegrove: *6th Int. Conf. on Numerical Analysis of Weldability*, Graz-Seggau, Austria, Oct. 2001.
33. D. Moreno, J. Garrett, and J.D. Embury: *Intermetallics*, 1999, vol. 7, pp. 1001–09.
34. R. Pretorius, T.K. Marais, and C.C. Theron: *Mater. Sci. Eng.*, 1993, vol. R10, pp. 1–83.
35. P. Xue, B.L. Xiao, D.R. Ni, and Z.Y. Ma: *Mater. Sci. Eng.*, 2010, vol. A527, pp. 5723–27.
36. H. Xu, C. Liu, V.V. Silberschmidt, and Z. Chen: *J. Electron. Mater.*, 2010, vol. 39 (1), pp. 124–31.